INTERNATIONAL JOURNAL OF STRUCTURAL CHANGES IN SOLIDS – Mechanics and Applications
Volume 2, Number 1, April 2010 , pp. 19-29

IJSCS

Constitutive Modeling of Anisotropic Finite-Deformation Hyperelastic Behaviors of Soft Materials Reinforced by Tortuous Fibers

Philip H Kao[1], Steven R. Lammers[1], Kendall Hunter[2], Kurt R. Stenmark[3,4], Robin Shandas[1,5], H. Jerry Qi[1,*]

[1]*Department of Mechanical Engineering, University of Colorado, Boulder, CO 80309*
[2]*Department of Pediatric Cardiology,*
[3]*Developmental Lung Biology Laboratory,*
[4]*Department of Pediatrics, University of Colorado Health Sciences Denver, CO*
[5]*Center for Bioengineering, University of Colorado, Anschutz Medical Campus, Aurora, CO*

Abstract

Many biological materials are composites composed of a soft matrix reinforced with stiffer fibers. These stiffer fibers may have a tortuous shape and wind through the soft matrix. At small material deformation, these fibers deform in a bending mode and contribute little to the material stiffness; at large material deformation, these fibers deform in a stretching mode and induce a stiffening effect in the material behavior. The transition from bending mode deformation to stretching mode deformation yields a characteristic J-shape stress-strain curve. In addition, the spatial distribution of these fibers may render the composite an anisotropic behavior. In this paper, we present an anisotropic finite-deformation hyperelastic constitutive model for such materials. Here, the matrix is modeled as an isotropic neo-Hookean material. "The behaviors of single tortuous fiber are represented by a crimped fiber model". The anisotropic behavior is introduced by a structure tensor representing the effective orientation distribution of crimped fibers. Parametric studies show the effect of fiber tortuosity and fiber orientation distribution on the overall stress-strain behaviors of the materials.

Keywords: Fiber reinforced composites; Constitutive model; Collagen fiber; Soft tissues.

1. Introduction

A biological tissue is a highly advanced material. It undergoes many cycles of deformation, and is purpose-made for each application. It is an intricate microstructural composite, composed of many types of proteins. One prevalent protein is collagen. Collagen is a stiff extracellular protein (Sasaki and Odajima, 1996(1,2); Cusack and Miller, 1979; Gosline, et al, 2002). It gives tendon its tensile stiffness (Sasaki and Odajima, 1996(2)), skin its strength (Holmstrand, et al, 1961), and bone its structure. In addition to collagen's intrinsic mechanical properties, the microstructural arrangement of collagen in tissues determines the mechanical behavior (Billiar and Sacks, 2000; Cacho, et al, 2007; Comninou and Yannas, 1976; Gasser, et al, 2006). In tendon the collagen is highly aligned to the direction of loading (Vidal and Mello, 2009), which provides its stiffness and strength. In skin the fibers are not highly aligned (Osaki, 1999), allowing the tissue to extend and undergo large deformations before rupturing. Microfibrillar collagen in tissues arranges into bundles, termed collagen fiber bundles (CFB) (Elbischger, et al, 2006). Because the collagen fibers have finite thickness, and are cross-linked within the bundles, it has been speculated that collagen fibers have a finite bending stiffness (Basu and Lardner, 1985; Buckley, et al, 1980). These fiber bundles are tortuous in the material unloaded state. As the tissue is loaded, the fiber bundles straighten and begin to bear load. This latent engagement allows the tissue to limit distension in order to avoid damaging the softer, weaker matrix proteins. The degree of tortuosity determines the distensibility of the tissue before it stiffens.

The effect of fiber orientations on the behavior of the tissue is tantamount to that of the tortuosity and bending stiffness of CFB. Most fiber reinforced tissue has an anisotropic nature, given that different tissues perform specific functions in the body. CFB are oriented in different directions, according to the function of the tissue. In example, artery

[*]Email: qih@colorado.edu

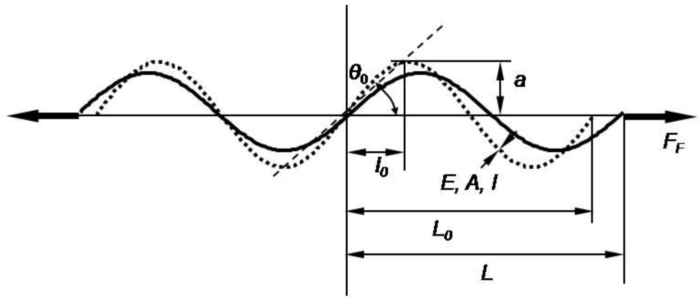

Figure 1: Schematic of crimped fiber model. The dotted line is the undeformed fiber configuration and the solid line is the deformed fiber configuration.

tissue has fibers arranged in the axial-circumferential polar plane to limit inflational and axial deformation. This anisotropic arrangement can be as complex as orthotropic. A constitutive model must then take into account material symmetry and degree of anisotropy.

This paper presents a two-part constitutive model, representing CFB and other matrix proteins. The CFB portion of the model uses a distributed CFB orientation as in (Gasser, et al, 2006), but also incorporates a second tunable axis for the orientation distribution. CFB are modeled as sinusoidal elastic beams which behave linear elastically, as was found by (Sasaki and Odajima, 1996(1)). This approach eschews the use of an engagement distribution function, which lowers model complexity. The second portion of the model uses an isotropic neo-Hookean constitutive formulation to represent the matrix behavior.

2. Modeling

2.1 *Modeling an Individual Collagen Fiber Bundle*

Here, we assume that the tortuous fiber can be represented by planar sinusoid-shaped beam, as was adopted previously for artery tissue (Basu and Lardner, 1985; Buckley, et al, 1980; Garikipati, et al, 2008). (Comninou and Yannas, 1976) developed a constitutive model for tendons consisting of sinusoidal collagen fiber bundles, termed crimped fibers. In their analysis, only small stretches and small-amplitude fiber crimp were considered. In this section of the paper, the crimped fiber model is extended to nonlinear stretch behavior. The fiber has a given elastic modulus, E, cross-sectional area, A, second moment of inertia, I, radius of gyration R, period $2\pi/b=4l_0$ and amplitude a as shown in Figure 1. From Figure 1, the six parameters, A, E, a, R, l_0 and I can be further simplified to four parameters: the modulus, E, the cross-sectional area, A, the ratio between bending rigidity and extensional stiffness, $R^2/l_0^2 = 4I/Al_0^2$, and another specifying the geometry of the fiber, $\bar{\theta}_0 = \operatorname{atan}(2ab/\pi)$. The undeformed and deformed contour lengths of the fiber are denoted as L_0^C, and L^C, respectively. The projected length of the undeformed fiber is L_0 and the deformed is L. It is important to understand the difference between the projected length and the contour length, as the average stretch internal to the fiber, defined as $\lambda = L^C/L_0^C$, gives rise to the force, and the apparent stretch, defined as $\lambda_F = L/L_0$, relates to the overall material deformation.

The undeformed beam can be described by

$$y = a\sin bx\,. \tag{1}$$

The contour length of the undeformed beam is

$$L_0{}^C = \sqrt{1+a^2b^2}\,\mathcal{E}\left(\sqrt{\frac{a^2b^2}{1+a^2b^2}}\right)L_0, \tag{2}$$

where $\mathcal{E}(.)$ is the complete elliptic integral of the second kind. Using the linearization of error $O(a^3b^3/3)$ applied by (Comninou and Yannas, 1976), under the application of the tensile load, F_F, the beam is assumed to deform to a sinusoidal shape with smaller amplitude but longer wavelength, expressed as

$$y = a\lambda_A \sin\frac{b}{\lambda_F}x\,, \tag{3}$$

where λ_A is the ratio of the current amplitude to the original amplitude, calculated as

$$\lambda_A = \frac{b^2}{\omega^2 + b^2}, \tag{4}$$

where ω relates the bending stiffness contribution of the beam and is calculated as

$$\omega^2 = (\lambda - 1)\frac{4}{R^2}\lambda . \tag{5}$$

R is the radius of gyration for the cross section of the beam. The contour length of the deformed beam can be calculated (see Appendix for detailed derivation) as

$$L^C = \sqrt{1 + \frac{\lambda_A{}^2 a^2 b^2}{\lambda_F{}^2}}\,\mathcal{E}\left(\sqrt{\frac{a^2b^2}{\frac{\lambda_F{}^2}{\lambda_A{}^2} + a^2b^2}}\right) L . \tag{6}$$

The relationship governing the stretch in the fiber compared to the apparent stretch is

$$\lambda = \sqrt{\frac{1 + \frac{\lambda_A{}^2}{\lambda_F{}^2} a^2 b^2}{1 + a^2 b^2}}\;\frac{\mathcal{E}\left(\sqrt{\frac{a^2b^2}{\frac{\lambda_F{}^2}{\lambda_A{}^2} + a^2b^2}}\right)}{\mathcal{E}\left(\sqrt{\frac{a^2b^2}{1 + a^2b^2}}\right)}\lambda_F . \tag{7}$$

Eq. (7) can be linearized with the same order of error as before, then rewritten in terms of the apparent fiber stretch, λ_F, and the material stretch, λ, by substituting the relationships, giving

$$\lambda_F = \lambda \frac{1 + a^2b^2/4}{1 + a^2b^2/4\left[4\lambda(\lambda - 1)(Rb)^{-2} + 1\right]^{-1}} . \tag{8}$$

Eq. (8) is rewritten in terms of the two fiber geometry parameters: R / l_0, $\overline{\theta}_0$

$$\lambda_F = \lambda \frac{1 + \frac{\pi^2}{8}\tan^2\overline{\theta}_0^2}{1 + \frac{\pi^2}{8}\tan^2\overline{\theta}_0^2\left[\frac{16}{\pi^2}\lambda(\lambda - 1)\left(\frac{l_0}{R}\right)^2 + 1\right]^{-1}} . \tag{9}$$

Eq. (9) is solved for the material stretch, λ, at a given λ_F. Assuming the fiber behaves as a Hookean material, given the observed stretch, the force is calculated from the stress as

$$F_F = EA(\lambda - 1). \tag{10}$$

2.2. *Orthotropic Crimped Fiber Model*

Here, we consider a material deformation that can be represented by a deformation gradient $\mathbf{F}$. The right Cauchy-Green deformation tensor, **C**, and the finger tensor **b** are defined as

$$\mathbf{C} = \mathbf{F}^T\mathbf{F},\ \mathbf{b} = \mathbf{F}\mathbf{F}^T,\ \mathbf{F} = \frac{\partial \mathbf{x}}{\partial \mathbf{X}}, \tag{11}$$

where $\mathbf{x}$ and $\mathbf{X}$ are spatial and material coordinates of a material point, respectively. The second Piola-Kirchhoff stress tensor $\mathbf{S}$, the first Piola-Kirchhoff stress $\mathbf{P}$, and the Cauchy stress $\boldsymbol{\sigma}$ are

$$\mathbf{S} = 2\frac{\partial \psi}{\partial \mathbf{C}},\ \mathbf{P} = \mathbf{FS},\ \boldsymbol{\sigma} = J^{-1}\mathbf{FSF}^T, \tag{12}$$

where ψ is the strain energy density function and J is the determinant of the deformation gradient. It is convenient to represent the strain energy function in terms of the invariants of **C**. In the isotropic case,

$$\psi = \psi(I_1, I_2, J), \tag{13a}$$

where

$$I_1 = \operatorname{tr}(\mathbf{C})$$
$$I_2 = \frac{1}{2}\left[\operatorname{tr}(\mathbf{C})^2 - \operatorname{tr}(\mathbf{C}^2)\right]. \tag{13b}$$
$$J = \det(\mathbf{F})$$

In the incompressible case, we require $J = 1$, thus the strain energy depends only on the first and second invariants.

In the anisotropic case with one family of fibers, there are two additional invariants pertaining to the deformation of the fibers. If the fibers are aligned in the direction of $\mathbf{a}_0$ then the structure tensor is defined as (Spencer, 1971)

$$\mathbf{A}_0 = \mathbf{a}_0 \otimes \mathbf{a}_0, \tag{14}$$

and the invariants describing the deformation of the fiber family are

$$I_4 = \mathbf{C} : \mathbf{A}_0 . \; I_5 = \mathbf{C}^2 : \mathbf{A}_0 \tag{15}$$

The fourth invariant has a straightforward meaning, and can be calculated as

$$I_4 = \lambda_{\mathbf{a}}{}^2, \tag{16}$$

where $\lambda_{\mathbf{a}}$ is the fiber stretch, and the fifth invariant is related to how the fibers couple to shear deformations. In this analysis, we use a unit vector **a** to denote $\mathbf{a}_0$ in the current configuration. Thus, **a** is calculated as

$$\mathbf{a} = \frac{\mathbf{F}\mathbf{a}_0}{\left\|\mathbf{F}\mathbf{a}_0\right\|}. \tag{17}$$

In the case of two fiber families, there are five additional invariants of the deformation tensor. If the fibers are aligned in the directions of $\mathbf{a}_0$ and $\mathbf{g}_0$, the structure tensors characterizing these fiber families are

$$\mathbf{A}_0 = \mathbf{a}_0 \otimes \mathbf{a}_0, \; \mathbf{G}_0 = \mathbf{g}_0 \otimes \mathbf{g}_0. \tag{18}$$

In addition to the invariants from the transversely isotropic case, I_4 and I_5, there are three additional invariants. The first two are calculated similar to I_4 and I_5 as,

$$I_6 = \mathbf{C} : \mathbf{G}_0, \; I_7 = \mathbf{C}^2 : \mathbf{G}_0. \tag{19a}$$

The eighth and ninth invariants use both structure tensors from the fiber families, and are calculated as

$$I_8 = \operatorname{tr}(\mathbf{C}\mathbf{A}_0\mathbf{G}_0), \; I_9 = \operatorname{tr}(\mathbf{A}_0\mathbf{G}_0). \tag{19b}$$

If $\mathbf{a}_0$ and $\mathbf{g}_0$ are orthogonal to one another, the eighth invariant is identically zero, and thus does not enter in to the calculations. In the model presented in this paper, it is assumed that the tissue is incompressible, and does not depend on the invariants involving $\mathbf{C}^2$. Thus, we consider invariants I_1, I_4 and I_6 with the constraint that $J = 1$. The model strain energy density is the total of strain energies representing the collagen fiber bundles and the isotropic, neo-Hookean material,

$$\psi = \psi_{NH} + \psi_{CF}, \tag{20a}$$

where the subscripts NH and CF denote the neo-Hookean and crimped fiber portions respectively. This linear superposition of strain energy density allows us to calculate the stresses as

$$\mathbf{S} = \mathbf{S}^{El} + \mathbf{S}^{CF}. \tag{20b}$$

If we consider the extension of a single fiber, the total energy is given by

$$\psi_F(\lambda_F) = A_F L_F \int_1^{\lambda_F} P_F d\lambda, \tag{21}$$

where P_F is the nominal stress in a fiber. The quantity A_F can be brought into the integral, and rewritten in terms of the force generated by the fiber as

$$\psi_F(\lambda_F) = L_F \int_1^{\lambda_F} F_F d\lambda. \tag{22}$$

It is important to note that Eq. (22) defines the total energy of the fiber, not a strain energy density.

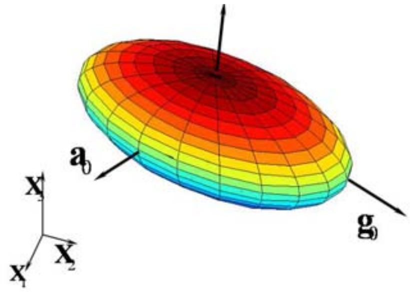

Figure 2: The ellipsoidal structure tensor, which shows how the structure tensor transforms unit vectors. A longer dimension indicates a higher concentration of fibers in that direction. a_0 and g_0 are not aligned with the global coordinate system, but in the model, are allowed to be aligned to whichever preferential directions the tissue may have.

To consider orthotropic material behaviors, a three-dimensional structure tensor, with two orthogonal directions and one isotropic component is used to characterize the material. As with the distributed collagen fiber orientation method of modeling used previously (Gasser, et al, 2006) a three-dimensional structure tensor is utilized to characterize the orientational distribution of the collagen fiber bundles. Unlike the method employed by (Gasser, et al, 2006) the structure tensor used here has two orthogonal groups of fibers, forming the major axes of an ellipsoid with tunable shape in all three major directions. The vectors $\mathbf{a_0}$ and $\mathbf{g_0}$ are aligned with the preferential directions of the fibers in the tissue in question. The structure tensor then takes the form

$$\mathbf{H}_0 = \frac{\kappa+\gamma-1}{3}\mathbf{I} + (1-\kappa)\mathbf{a_0}\otimes\mathbf{a_0} + (1-\gamma)\mathbf{g_0}\otimes\mathbf{g_0}. \tag{23}$$

This structure tensor can be visualized as an ellipsoid with trace of 1, as in Figure 2. The structure tensor in the current configuration is denoted as

$$\mathbf{H} = \mathbf{F}\mathbf{H}_0\mathbf{F}^T. \tag{24}$$

The structure parameters, κ and γ, must satisfy the requirements that $0 \le \kappa \le 1$, $0 \le \gamma \le 1$, and $\kappa+\gamma \ge 1$ in order to ensure that none of the major dimensions of the structure tensor become negative. As with the model introduced by (Gasser, et al, 2006; and Spencer, 1984), the stretch experienced by a fiber is related to the structure tensor by $\lambda_F^2 = \mathbf{H}_0 : \mathbf{C}$. This can be written in terms of the invariants,

$$\lambda_F = \sqrt{\mathbf{H}_0 : \mathbf{C}} = \sqrt{\frac{\kappa+\gamma-1}{3}I_1 + (1-\kappa)I_4 + (1-\gamma)I_6}. \tag{25}$$

The strain energy density function is given by

$$\psi_{CF} = K\psi_F(\lambda_F). \tag{26}$$

In general, for a material dependent on the first, fourth and sixth invariants, the stress is given by

$$\mathbf{S} = 2\frac{\partial\psi}{\partial I_1}\mathbf{I} - p\mathbf{C}^{-1} + 2\frac{\partial\psi}{\partial I_4}\mathbf{a}_0\otimes\mathbf{a}_0 + 2\frac{\partial\psi}{\partial I_6}\mathbf{g}_0\otimes\mathbf{g}_0, \tag{27a}$$

Where

$$\begin{aligned}
\frac{\partial\psi_{CF}}{\partial I_1} &= \frac{1}{2}KF_F(\lambda_F)\lambda_F^{-1}\left(\frac{\kappa+\gamma-1}{3}\right)\\
\frac{\partial\psi_{CF}}{\partial I_4} &= \frac{1}{2}KF_F(\lambda_F)\lambda_F^{-1}(1-\kappa)\\
\frac{\partial\psi_{CF}}{\partial I_6} &= \frac{1}{2}KF_F(\lambda_F)\lambda_F^{-1}(1-\gamma)
\end{aligned}, \tag{27b}$$

Where K is the fiber number density. Using Eqs. (27a, b), the stress is

$$\mathbf{S}^{CF} = K\frac{F_F(\lambda_F)}{\lambda_F}\left[\left(\frac{\kappa+\gamma-1}{3}\right)\mathbf{I} + (1-\kappa)\mathbf{a}_0\otimes\mathbf{a}_0 + (1-\gamma)\mathbf{g}_0\otimes\mathbf{g}_0\right] - p\mathbf{C}^{-1}. \tag{28}$$

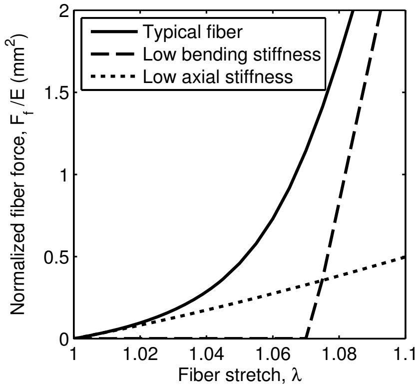

Figure 3: The normalized force-extension behavior for three cases of fibers is shown. The fiber force, f is normalized by the Young's modulus, E. The solid line shows a typical force-extension behavior of a crimped fiber. The dashed line is shown with very small bending stiffness. The dotted line shows a crimped fiber where the extensional stiffness is very low.

2.3. Complete Model for Composites

The model strain energy is the total of the strain energies representing the collagen fiber bundles and the elastin network weighted by its volume fraction,

$$\psi = f_{El}\psi_{El} + \psi_{CF}\,. \tag{29}$$

This is a simple but effective treatment for composites and ignores the interaction between fibers and matrix. Since the collagen fiber bundle model already contains a fiber areal number density, K, Eq. (28) does not have a volume fraction for collagen fiber bundle energy density. In addition, it is possible to lump the volume fraction f_{El} with the elastin shear modulus. This linear superposition of strain energy allows us to calculate the stresses as

$$\mathbf{S} = \mathbf{S}^{El} + \mathbf{S}^{CF}\,, \tag{30}$$

which can be rewritten as

$$\mathbf{S} = \mu\mathbf{I} + K\frac{F_F\left(\lambda_F\right)}{\lambda_F}\mathbf{H}_0 - p\mathbf{C}^{-1}\,. \tag{31}$$

Because A and K together determine the total area of the collagen fibers per unit material area, it is advantageous to lump the two together, KA. Thus, in total, there are seven parameters to consider: the elastic network isotropic shear modulus, μ ; three parameters for the collagen fiber bundles: intrinsic Young's Modulus, E, fiber shape, $\bar{\theta}_0$, and normalized radius of gyration, R/l_0; one pertaining to collagen fibers per unit material area, KA; and two for the orthotropic structure tensor: the major axis $\mathbf{a}_0$, κ, and the second major axis $\mathbf{g}_0$, γ. In order to simplify the model further, for this paper, the modulus of collagen was chosen to be in the range of previous work(Sasaki and Odajima, 1996; Cusack and Miller, 1979; Harley, et al, 1977; Zulliger, et al, 2004), with a value of 10 GPa.

3. Results

In the following, we evaluate the model behavior by investigating the stress-strain response of a material under uniaxial loading conditions. First, the single crimped fiber is analyzed for the contribution of the bending stiffness and axial stiffness. Second, the stress-stretch response of the model under uniaxial loading is developed. Lastly, we conduct parametric studies to observe the effects of structural parameters on the model predictions.

3.1. Single Fiber Extensional and Bending Stiffness

To better understand the fiber behavior, three cases of fiber parameters were studied. First, the force-extension behavior of a typical crimped fiber is shown in Figure 3. This typical fiber has a non-zero bending stiffness, where its bending stiffness is seen by its non-zero tangent slope at low stretch. The second and the third represent the two extremes. In the second case, the force extension behavior of a fiber with zero bending stiffness is plotted. It is seen that there is zero force until the fiber is straight, where the force increases linearly at the extensional stiffness. This ultimate stiffness is the same as that of the typical fiber. In the third case, the fiber has low extensional stiffness compared to the bending stiffness. This fiber's behavior is comparable to the typical fiber at stretches close to 1, but behaves linearly as the stretch is increased. This linear behavior is because the amplitude of the fiber remains constant as it is stretched, giving a constant stiffness. This is a somewhat fictitious response, though, as a fiber with low extensional stiffness also has low bending stiffness. The discrepancy between the full model and the sum of the two extremes is due to a convoluting effect of the extensional stiffness on the total fiber behavior, thus causing a deviation from the bending stiffness dominant fiber response.

3.2 Model Simulations of Uniaxial Deformation

Material point simulations were performed using the model with varying parameters. For these simulations, $\mathbf{a}_0$ and $\mathbf{g}_0$ were aligned to the global direction vectors $\mathbf{X}_1$ and $\mathbf{X}_2$ respectively. Applying the load in the 1-direction, S_{11}, one can solve for the uniaxial stress by applying the appropriate boundary conditions of $S_{22}=S_{33}=0$ and the incompressibility constraint. Taking the full orthotropic model, with the stress applied in the 1-direction,

$$\begin{aligned} S_{11} &= \mu + K\frac{F_F(\lambda_F)}{\lambda_F}\left(\frac{-2\kappa+\gamma+2}{3}\right) - p\frac{1}{\lambda^2} \\ S_{22} &= \mu + K\frac{F_F(\lambda_F)}{\lambda_F}\left(\frac{\kappa-2\gamma-2}{3}\right) - p\frac{1}{\lambda_2^2} = 0 \quad , \\ S_{33} &= \mu + K\frac{F_F(\lambda_F)}{\lambda_F}\left(\frac{\kappa+\gamma-1}{3}\right) - p\left(\lambda\lambda_2\right)^2 = 0 \end{aligned} \tag{32}$$

where

$$\lambda_F = \sqrt{\frac{\kappa+\gamma-1}{3}\left(\lambda^2+\lambda_2{}^2+\frac{1}{\lambda^2\lambda_2{}^2}\right)+(1-\kappa)\lambda^2+(1-\gamma)\lambda_2{}^2}\,. \tag{33}$$

Using $S_{33}=0$, we can solve for the Lagrange multiplier associated with the incompressibility constraint, p, as

$$p = \frac{\mu + K\dfrac{F_F(\lambda_F)}{\lambda_F}\left(\dfrac{\kappa+\gamma-1}{3}\right)}{\left(\lambda\lambda_2\right)^2}\,. \tag{34}$$

Combining this with S_{22}, we obtain the expression

$$\lambda_2{}^4 = \frac{\mu + K\dfrac{F_F(\lambda_F)}{\lambda_F}\left(\dfrac{\kappa+\gamma-1}{3}\right)}{\lambda^2\left[\mu + K\dfrac{F_F(\lambda_F)}{\lambda_F}\left(\dfrac{\kappa-2\gamma-2}{3}\right)\right]}\,. \tag{35}$$

This can be solved numerically for λ_2 and λ_F given λ. Once λ_2 and λ_F are obtained, the uniaxial stress can be calculated. For uniaxial tests in the 2-direction where S_{22} is controlled, the process is similar, but with $S_{11}=0$.

3.3 Full Model Behavior

Here, the effects of the crimped fiber orthotropic model parameters are studied. The parameters can be tuned to achieve a certain behavior. Besides having high flexibility in modeling anisotropy and engagement, the model produces a basic shape of the stress-stretch curves that is consistent with the J-shape seen in many soft biological tissues.

Figures 4 and 5 show the stress-stretch curves for varying one parameter and holding the others constant. In these figures, λ_1 and λ_2 correspond to the $\mathbf{X}_1$ and $\mathbf{X}_2$ stretches, respectively. All stresses are the first Piola-Kirchhof stress. In Figure 4(a-c), the uniaxial material response is shown for the orthotropic crimped-fiber model, showing the effect of changing the model parameters pertaining to fiber orientations. In addition to the crimped fiber model, the isotropic neo-Hookean model response is also plotted for reference. For each set of parameters, the resultant uniaxial behaviors along the two orthogonal directions are shown.

Figure 4(a) shows the case for $\gamma=\kappa$. The material demonstrates an isotropic behavior with a characteristic J-shape. The transition from the initial low stiffness to the ultimate high stiffness can be roughly represented by a transition strain, or engagement strain (Lammers, et al, 2008). Although a more sophisticated definition of engagement strain is provided in our recent study (Lammers, et al, 2008), for the purpose of illustration of model behavior, we

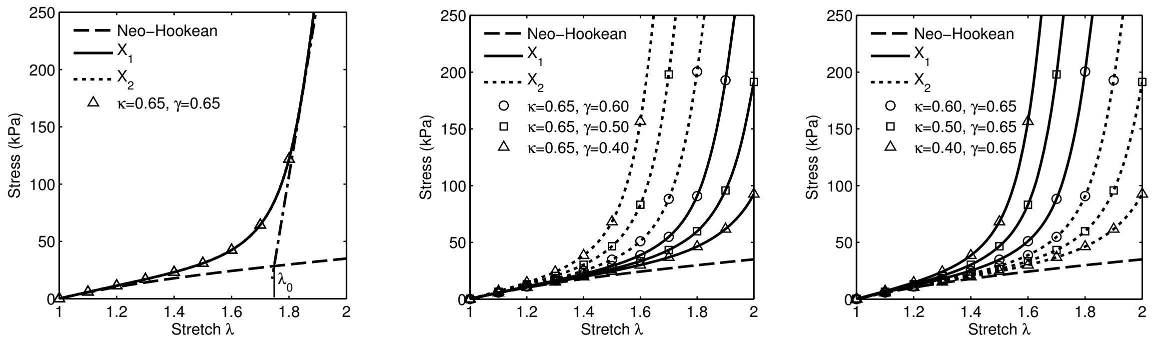

(a) (b) (c)

Figure 4: A parametric study varying κ and γ. A) It is seen that when $\kappa = \gamma$, the behavior is transversely isotropic; the uniaxial stress-stretch curves lay on top of one another. B) As γ is decreased in relation to κ the $\mathbf{X}_2$ behavior becomes increasingly stiffer than the $\mathbf{X}_1$ direction. The $\mathbf{X}_1$ directions are in solid lines and the $\mathbf{X}_2$ directions are in dotted lines. C) As κ is decreased in relation to γ, the degree of anisotropy is increased, with the $\mathbf{X}_1$ direction becoming significantly stiffer than the $\mathbf{X}_2$ direction. Here μ=20 kPa, KA=1x10^{-3}, E=10GPa, $\overline{\theta}_0$=27°, R/l_0 =0.05.

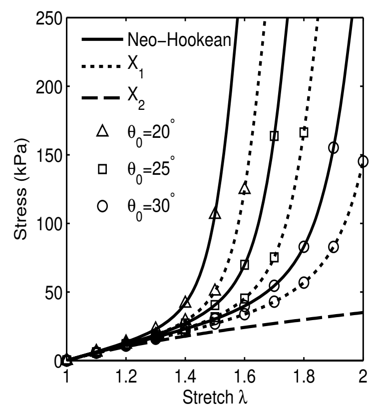

Figure 5: Results for the crimped fiber model, showing the effect of changing crimped fiber parameter $\overline{\theta}_0$. The stress-strain behaviors in $\mathbf{X}_1$ directions are in solid lines and in the $\mathbf{X}_2$ directions are in dotted lines. As $\overline{\theta}_0$ increases, the engagement strain, where the material stiffens, moves rightward. It also decreases the overall stiffness, as the contour length is increased. Here μ=20 kPa, KA=1x10^{-3}, E=10GPa, R/l_0 =0.05, κ=0.60 and γ=0.65.

simply use the intersection of the linear extrapolations of low and high stretch portions of the stress-stretch curve to define the engagement strain, as shown as λ_0 in Figure 4(a). The neo-Hookean behavior is also shown in Figure 4(a) for comparison. Figure 4(b) shows the change in material behavior due to changes in γ. A lower value for γ corresponds to fiber alignment in the $\mathbf{X}_2$ direction. Decreasing γ (or fiber orientation prefers $\mathbf{X}_2$ direction) causes the engagement in the $\mathbf{X}_2$ direction to occur at a smaller stretch and in the $\mathbf{X}_1$ at a larger stretch. This is because, as illustrated in the previous study using the Arruda-Boyce eight chain model (1993) polymer chains, when they are in a network, can accommodate large deformation through rigid body rotation. Therefore, as the fiber is oriented toward $\mathbf{X}_2$ direction, the fiber can rotate more toward $\mathbf{X}_1$ direction to accommodate a larger stretch in the $\mathbf{X}_1$ direction and can rotate less toward $\mathbf{X}_2$ direction to accommodate deformation in the $\mathbf{X}_2$ direction. From the fiber point of view, the stretch mode is engaged at a larger stretch in the $\mathbf{X}_1$ direction than it does in the $\mathbf{X}_2$ direction. Figure 4(c) shows the change in material behavior due to changing κ while holding all other parameters constant causes an observed change in the anisotropy of the collagen component. Figure 4(c) shows the opposite trend of Figure 4(b). As κ decreased, the fiber becomes more oriented toward $\mathbf{X}_1$ direction, which causes a smaller engagement strain in the $\mathbf{X}_1$ direction and larger engagement strain in the $\mathbf{X}_2$ direction.

The change in material behavior due to a change in $\overline{\theta}_0$, as in Figure 5, is observed in both the ultimate stiffness and engagement stretch. Increasing $\overline{\theta}_0$ directly causes an increase in the engagement strain. In addition to increasing the

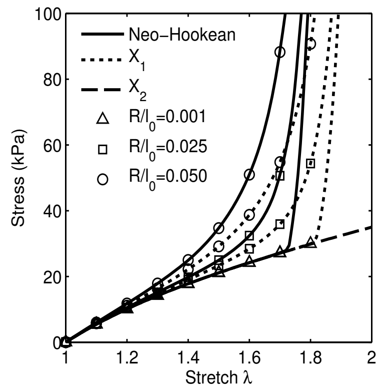

Figure 6: Results for the crimped fiber model, showing the effect of changing crimped fiber parameter R/l_0 . As the radius of gyration is changed, it causes the transition to broaden and become more gradual. Here the parameters held constant are μ=20 kPa, KA=1x10^{-3}, E=10GPa, $\bar{\theta}_0$ =27°, κ=0.55 and γ=0.65.

engagement stretch, the ultimate stiffness is decreased. This is, as stated earlier, due to the increased contour length of the beam with constant end-to-end distance. It may appear that the degree of anisotropy is increased with increasing $\bar{\theta}_0$, but the perceived increase in the degree of anisotropy is due only to the increased stretch at which engagement occurs.

The effect of R/l_0 on behavior is shown in Figure 6. At low values of R/l_0 , there is little contribute from the fiber, as shown in Figure 6, the initial stiffness is given by neo-Hookean matrix. The stiffness rapidly increases and becomes linear quickly above the engagement stretch. At higher values, it is seen that there is some low-stretch stiffness due to the fibers and the transition to the fully-developed stiffness is more gradual.

4. Conclusions

An orthotropic constitutive model for a composite with an isotropic soft matrix reinforced by tortuous fibers was presented. Here, the matrix was modeled as an isotropic neo-Hookean material. The tortuous fiber wass modeled by a crimped fiber model, which considered the fiber as a planar sinusoidal linear elastic beam. The anisotropic behavior was introduced by a structure tensor representing the effective orientation distribution of crimped fibers. The model described the transition of the material stress-strain behavior from an initial low stiffness at low stretch ratio to a very stiff response at high stretch ratio, a characteristic behavior of many biological soft tissues. The model has relatively low complexity, due to the flexibility afforded by the sinusoidal crimped fiber model and the ellipsoidal structure tensor used to represent the orthotropic behavior of the material.

Acknowledgement

This work was supported by grants from the NIH (T32-HL072738, SCCOR-HL081506, K24-HL084923).

Appendix: Derivation of contour length of the undeformed and deformed sinusoidal beam

To calculate the contour length of the beam, we find the incremental arc length *ds* for a given differential length *dx* and subsequent differential change *dy*, with Eq. (1) as the function,

$$\begin{aligned}\frac{ds^2}{dx^2} &= \left(\frac{dy}{dx}\right)^2 + 1 \\ \frac{ds}{dx} &= \sqrt{a^2b^2\cos^2 bx + 1} \\ ds &= \sqrt{a^2b^2\cos^2 bx + 1}dx\end{aligned} \quad . \tag{A1}$$

Integrating along the length, we obtain

$$s = \frac{\sqrt{1+a^2b^2}}{b}\mathcal{E}\left[bx, \sqrt{\frac{a^2b^2}{1+a^2b^2}}\right], \tag{A2}$$

Integrating only to the first quarter wavelength is necessary, as the quarter wavelengths shapes are similar, we obtain

$$s = \sqrt{1+a^2b^2}\,\mathcal{E}\left(\sqrt{\frac{a^2b^2}{1+a^2b^2}}\right)x\,. \tag{A3}$$

For the deformed beam whose shape is described by Eq. 16, the arc length s is calculated as

$$s = \frac{\lambda_F}{b}\sqrt{1+\frac{\lambda_A{}^2a^2b^2}{\lambda_F{}^2}}\,\mathcal{E}\left[\frac{bx}{\lambda_F}, \sqrt{\frac{\lambda_A{}^2a^2b^2}{\lambda_F{}^2+\lambda_A{}^2a^2b^2}}\right], \tag{A4}$$

and for the first quarter wavelength is

$$s = \sqrt{1+\frac{\lambda_A{}^2a^2b^2}{\lambda_F{}^2}}\,\mathcal{E}\left[\sqrt{\frac{\lambda_A{}^2a^2b^2}{\lambda_F{}^2+\lambda_A{}^2a^2b^2}}\right]x\,. \tag{A5}$$

References:

Arruda, E.M. and M.C. Boyce, A 3-Dimensional Constitutive Model for the Large Stretch Behavior of Rubber Elastic-Materials. Journal of the Mechanics and Physics of Solids, 1993. **41**(2): p. 389-412.

Basu, A.J. and T.J. Lardner, Deformation Of A Planar Sinusoidal Elastic Beam. Zeitschrift Fur Angewandte Mathematik Und Physik, 1985. **36**(3): p. 460-474.

Billiar, K.L. and M.S. Sacks, Biaxial mechanical properties of the natural and glutaraldehyde treated aortic valve cusp - Part I: Experimental results. Journal of Biomechanical Engineering-Transactions of the Asme, 2000. **122**(1): p. 23-30.

Buckley, C.P., D.W. Lloyd, and M. Konopasek, On the Deformation of Slender Filaments with Planar Crimp: Theory, Numerical Solution and Applications to Tendon Collagen and Textile Materials. Proceedings of the Royal Society of London. A. Mathematical and Physical Sciences, 1980. **372**(1748): p. 33-64.

Cacho, F., et al., A constitutive model for fibrous tissues considering collagen fiber crimp. International Journal of Non-Linear Mechanics, 2007. **42**(2): p. 391-402.

Comninou, M. and I.V. Yannas, Dependence of Stress-Strain Nonlinearity of Connective Tissues on Geometry of Collagen-Fibers. Journal of Biomechanics, 1976. **9**(7): p. 427-433.

Cusack, S. and A. Miller, Determination Of The Elastic-Constants Of Collagen By Brillouin Light-Scattering. Journal Of Molecular Biology, 1979. **135**(1): p. 39-51.

Elbischger, P.J., et al. Modeling and characterizing collagen fiber bundles. 2006. Piscataway, NJ, USA: IEEE.

Garikipati, K., S. Goktepe, and C. Miehe, Elastica-based strain energy functions for soft biological tissue. Journal Of The Mechanics And Physics Of Solids, 2008. **56**(4): p. 1693-1713.

Gasser, T.C., R.W. Ogden, and G.A. Holzapfel, Hyperelastic modelling of arterial layers with distributed collagen fibre orientations. Journal of the Royal Society Interface, 2006. **3**(6): p. 15-35.

Gosline, J., et al., Elastic proteins: biological roles and mechanical properties. Philosophical Transactions of the Royal Society of London Series B-Biological Sciences, 2002. **357**(1418): p. 121-132.

Harley, R., et al., Phonons And Elastic-Moduli Of Collagen And Muscle. Nature, 1977. **267**(5608): p. 285-287.

Holmstrand, K., J.J. Longacre, and G.A. Destefano, The Ultrastructure of Collagen in Skin, Scars and Keloids. Plastic and Reconstructive Surgery, 1961. **27**(6): p. 597-607.

Lammers, S.R., et al., Changes in the structure-function relationship of elastin and its impact on the proximal pulmonary arterial mechanics of hypertensive calves. American Journal of Physiology-Heart and Circulatory Physiology, 2008. **295**(4): p. H1451-H1459.

Osaki, S., Distribution map of collagen fiber orientation in a whole calf skin. The Anatomical Record, 1999. **254**(1): p. 147-152.

Sasaki, N. and S. Odajima, Elongation mechanism of collagen fibrils and force-strain relations of tendon at each level of structural hierarchy. Journal of Biomechanics, 1996. **29**(9): p. 1131-1136.

Sasaki, N. and S. Odajima, Stress-strain curve and Young's modulus of a collagen molecule as determined by the X-ray diffraction technique. Journal of Biomechanics, 1996. **29**(5): p. 655-658.

Spencer, A.J.M., Constitutive theory for strongly anisotropic solids, in Continuum Theory of the Mech of Fibre-Reinf Compos. 1984, Springer Verlag: Vienna, Austria. p. 1.

Spencer, A.J.M., Theory of invariants, in *Continuum Physics* volume 1: Mathematics. 1971, Academic: London, UK. p. 239.

Vidal, B.D. and M.L.S. Mello, Structural organization of collagen fibers in chordae tendineae as assessed by optical anisotropic properties and Fast Fourier transform. Journal of Structural Biology, 2009. **167**(2): p. 166-175.

Zulliger, M.A., et al., A strain energy function for arteries accounting for wall composition and structure. Journal of Biomechanics, 2004. **37**(7): p. 989-1000.